π electronic structure of octahedral trivalent cages consisting of hexagons and squares

S. Compernolle and A. Ceulemans
Laboratorium voor Kwantumchemie, Katholieke Universiteit Leuven, Celestijnenlaan 200F, B-3001 Heverlee, Belgium
(Received 2 December 2004; published 20 May 2005)

A zone-folding construction is applied to the honeycomb lattice band structure to yield explicit expressions for the Hückel π-molecular orbitals, energies and symmetries of trivalent polyhedra consisting of hexagons and squares [(4,6) cages] with octahedral symmetry. The A_1, A_2, and E representations are accessible in this way, but not the T_1 and T_2 representations. Therefore, we have also performed numerical Hückel calculations on a large set of cages. A clear distinction in electronic structure between leapfrog, nonleapfrog type 1 and nonleapfrog type 2 cages is revealed. The results are relevant both for carbon cages and alternating boron-nitride cages. Quantum chemical calculations on C_{24}, C_{56}, C_{72}, and $B_{36}N_{36}$ confirm the results.

DOI: 10.1103/PhysRevB.71.205407 PACS number(s): 73.22.−f, 73.20.At, 36.40.−c, 36.20.Kd

I. INTRODUCTION

In this work we are concerned with (4,6) cages, which are defined as trivalent cages consisting of hexagons and squares. For a cage with v atoms the number of squares always equals 6, while the number of hexagons is given by $v/2-4$. In the carbon family, the most famous trivalent cage type is of course the fullerene, defined as a carbon cage consisting of 12 pentagonal faces and $v/2-10$ hexagonal faces. Therefore we can call it also a (5,6) cage. For most stable fullerenes ($v=60, v\geqslant 70$) it has been found that they obey the isolated pentagon rule (IPR): no two pentagons can share a bond.[1,2] But trivalent cages with $v<60$ or $60<v<70$ must necessary violate the IPR rule *or* have faces other than pentagons and hexagons. Several theoretical studies[3–10] indicate that one or two four-membered rings can play a part in these fullerenes. Qian *et al.*[11] synthesized a nonclassical fullerene C_{62} with one four-membered ring. So squares can be important in carbon cages, but for a cage consisting of only squares and hexagons, one has to look for another starting material instead of carbon.

Several alternant boron-nitride (BN) analogs to carbon structures have been synthesized, for example analogs to benzene,[12] graphite,[13] and diamond[14] and more recently to nanotubes[15,16] and nanocages.[17,18] For the latter, two distinct plausible classes have been investigated theoretically. The first class consists of (5,6) cages like the classical fullerenes which necessarily have some unfavorable homonuclear B-B or N-N bonds.[19] The second class are (4,6) cages[20–27] with a rigorous BN alternation that compensates for the strain-inducing squares. Theoretical studies disagree about which class delivers the most stable cages.[28–31] A systematic study has shown that within the class of the (4,6) BN cages, the ones without adjacent squares are the most stable.[32]

In this study we will focus on octahedral (4,6) cages—both carbon and BN structures—as defined by Zhu *et al.*[20,21] These structures are in their BN form often of special stability compared to other (4,6) BN cages.[27,33] We will show that analytical expressions for nondegenerate or doubly degenerate eigenvalues and molecular orbitals (MO) can be obtained within the Hückel approximation, by means of a zone-folding procedure similar to that applied previously to nanotubes,[34] nanotori,[35] and (3,6) cages.[36]

The paper is organized as follows. Section II explains how the Hückel spectra of both carbon and BN (4,6) cages are related to the eigenvalues of the adjacency matrix of the underlying graph. Section III introduces the central geometrical relationship by which an octahedral (4,6) cage can be unfolded into a (2,6) cage which in turn can provide a covering of the honeycomb lattice. This relationship defines a zone-folding procedure which generates analytical expressions for MOs transforming according to the A_1, A_2 and E irreducible representations of the octahedral cage. The explicit derivation of these MOs is done in Sec. IV and of their symmetries in Sec. V. Section VI focuses on the MOs of the $A+E$ group that are close to nonbonding. The MOs of symmetry T_1 and T_2 of a (4,6) cage cannot be obtained by the zone-folding method. Instead, we have performed numerical Hückel calculations on a large set of cages and the results are presented in Sec. VII. Section VIII compares the Hückel results with DFT-B3LYP calculations. The general conclusions are given in Sec. IX.

II. RELATION BETWEEN HÜCKEL SPECTRA OF C AND BN (4,6) CAGES

In the simple Hückel approximation, the Hamiltonian for carbon allotropes takes the following form:

$$\mathbf{H}_C = \alpha_C \mathbf{I} + \beta_{CC}\mathbf{A}, \tag{1}$$

with α_C the Coulomb integral and β_{CC} the hopping integral. As β_{CC} represents a bonding interaction we have $\beta_{CC}<0$. $\mathbf{I}$ is the unit matrix and $\mathbf{A}$ the connectivity matrix of the system, representing a graph. The orbital energies of $\mathbf{H}_C$ can be expressed in function of the eigenvalues λ of $\mathbf{A}$:

$$E_C = \alpha_C + \beta_{CC}\lambda, \tag{2}$$

while the eigenfunctions of $\mathbf{A}$ and $\mathbf{H}_C$ are the same. Each cage discussed here is an alternant: its vertices can be divided into two equal sets, black and white, such that every vertex of one set is only surrounded by members of the other.

As pointed out by Zhu *et al.*,[20] the Hamiltonian of a rigorously alternating BN allotrope is equal to

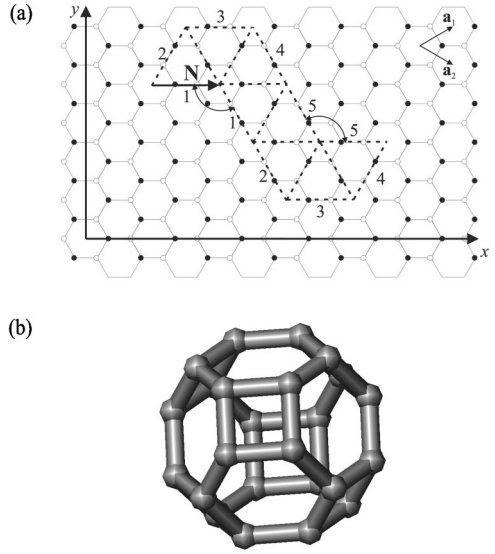

FIG. 1. Octahedral (4,6) cage, unfolded on the honeycomb plane (a) and in the folded state (b). $\mathbf{N}=n_1\mathbf{a}_1+n_2\mathbf{a}_2$ defines the cage. For the cage shown indices correspond to $n_1=1$ and $n_2=1$, and the number of carbon atoms is 24. The vectors $\mathbf{a}_1$ and $\mathbf{a}_2$ are the unit vectors of the honeycomb lattice.

$$\mathbf{H}_{\mathrm{BN}} = \mathbf{D} + \beta_{\mathrm{BN}}\mathbf{A}, \tag{3}$$

with $\mathbf{D}$ a diagonal matrix whose elements are α_{B} for a boron atom, which takes the place of a black vertex, and α_{N} for a nitrogen atom, which takes the place of a white vertex. The orbital energies of $\mathbf{H}_{\mathrm{BN}}$ are[20]

$$E_{\mathrm{BN}} = \alpha_{\mathrm{BN}} \pm \sqrt{\Delta^2 + \beta_{\mathrm{BN}}^2\lambda^2},$$

$$\alpha_{\mathrm{BN}} = \frac{\alpha_{\mathrm{B}} + \alpha_{\mathrm{N}}}{2},$$

$$\Delta = \frac{\alpha_{\mathrm{B}} - \alpha_{\mathrm{N}}}{2}. \tag{4}$$

Since λ^2 cannot be lower than zero, the minimal HOMO-LUMO gap of an alternating BN system is $2|\Delta|$, with Δ nearly the size of β_{BN}.[37]

We will from now on work only with the graph—i.e., black and white atoms each have the same diagonal element 0 in the connectivity matrix—and express the MO energies by the dimensionless quantity λ. E_{C} or E_{BN} can always be found by using Eqs. (2) and (4), respectively.

III. RELATIONSHIP BETWEEN THE EIGENVALUE PROBLEM OF OCTAHEDRALLY SYMMETRIC (4,6) CAGES, (2,6) CAGES AND TORI

An octahedrally symmetric (4,6) cage can be imagined as a honeycomb lattice inscribed on a master octahedron. The symmetry will be lowered to tetrahedral symmetry for a BN cage. Figure 1(a) shows a patch consisting of eight equilateral triangles drawn on the honeycomb lattice. Upon folding this patch an octahedrally symmetric (4,6) cage is obtained [Fig. 1(b)] as was described in Ref. 20. The cage is completely defined by the vector $\mathbf{N}$ along one edge of a constituent equilateral triangle

$$\mathbf{N} = n_1\mathbf{a}_1 + n_2\mathbf{a}_2, \tag{5}$$

with n_1, n_2 integers and $\mathbf{a}_1$, $\mathbf{a}_2$ the basis vectors of the honeycomb lattice,

$$\mathbf{a}_1 = a\left(\frac{\sqrt{3}}{2}\mathbf{e}_x + \frac{1}{2}\mathbf{e}_y\right),$$

$$\mathbf{a}_2 = a\left(\frac{\sqrt{3}}{2}\mathbf{e}_x - \frac{1}{2}\mathbf{e}_y\right), \tag{6}$$

where $a=\sqrt{3}\times r_{\mathrm{CC}}$, with r_{CC} the nearest neighbor distance. To construct all possibilities—omitting enantiomers—it is sufficient to consider $n_1 \geqslant n_2 \geqslant 0$. One can distinguish the following types:

$$n_2 = 0\text{: zigzag},$$

$$n_2 = n_1\text{: armchair},$$

$$n_1 - n_2 = 3q\text{: leapfrog},$$

$$n_1 - n_2 = 3q + 1\text{: nonleapfrog type 1},$$

$$n_1 - n_2 = 3q - 1\text{: nonleapfrog type 2}. \tag{7}$$

The first two definitions are similar to the ones commonly used for nanotubes.[34] A more general definition of leapfrogs and nonleapfrogs—not confined to octahedral (4,6) cages—can be found in Ref. 38. Zigzag and armchair cages have O_h symmetry while the other cages are chiral and have O symmetry. Considering BN cages, the symmetry is lowered to T_d for zigzag, T_h for armchair and T otherwise. Note that armchair cages are always leapfrogs. Profound differences in the electronic structure have often been encountered between leapfrog and nonleapfrog members of graphitic species, such as nanotubes,[34] fullerenes,[39] (3,6) cages,[36] and nanotori.[35] In the case of octahedral (4,6) cages, we will show that there are also important differences between nonleapfrogs of type 1 and type 2.

The number of vertices $v_{(4,6)}$ of the (4,6) cage is equal to

$$v_{(4,6)} = 8(n_1^2 + n_2^2 + n_1n_2). \tag{8}$$

The operations C_{4x}^2, C_{4y}^2 and C_{4z}^2—the three twofold rotational axes going through the square centers—can be used to construct a so-called (2,6) cage[40] corresponding to the original (4,6) cage with only $v_{(2,6)}=v_{(4,6)}/4$ vertices. First, one chooses two triangles of the master octahedron sharing a side, labeling them A and B, respectively. The other triangles can be related to these two by the operations C_{4x}^2, C_{4y}^2 and C_{4z}^2 and can also be labeled A or B in this way [Fig. 2(a)].

Each triangle A has now a triangle B as neighbor along each of its edges and vice versa. Let us take two neighboring triangles A and B and fold them together as shown in Fig. 2(b). The triangle A (B) is then "surrounded" by the triangle $B(A)$ along each of its edges in the same way as for Fig. 2(a).

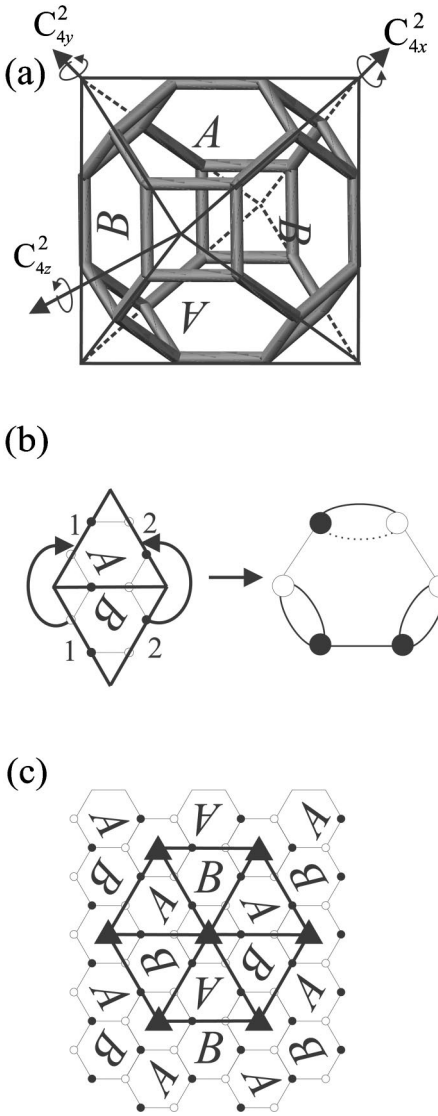

FIG. 2. (a) A folded octahedral (4,6) cage with the 8 master triangles labeled A and B in such a way that the resulting pattern is totally symmetric with respect to the operations C^2_{4x}, C^2_{4y}, and C^2_{4z}. (b) A (2,6) cage, defined by folding the two neighboring master triangles A and B, presented unfolded (left, sides with the same number should be glued together) and folded (right). (c) One can fill the plane—using as tile the pair of triangles from (b) (left)—to obtain the honeycomb plane with a pattern inscribed that is totally symmetric with respect to periodically placed C_3 axes—represented by black triangles—and periodic boundary conditions, represented by the hexagonal patch. Opposite sides of the hexagonal patch should be glued together.

So MOs of the (4,6) cage that are totally symmetric with respect to the three generators C^2_{4x}, C^2_{4y} and C^2_{4z} correspond to eigenfunctions of the (2,6) cage. These MOs have symmetry label A_1, A_2 or E (we limit ourselves to symmetry labels of the point group O in this section) and we call this group the $A+E$ group. The other MOs have symmetry label T_1 and T_2 (the T group).

The triangle pair A/B can further be used as a building block to fill the plane. Again, this can be done in such a way that each triangle A is surrounded by the triangle B along each of its edges and vice versa. The resulting structure is the honeycomb lattice with a pattern inscribed that is totally symmetric with respect to trigonal periodic boundary conditions, with periodically placed C_3 axes [Fig. 2(c)]. The periodic boundary conditions are represented by a hexagonal patch in Fig. 2(c); each pair of opposite sides of the patch defines a cyclic boundary condition. The patch consists of three A/B triangle pairs. By this construction, the center and the corners of the patch coincide with the centers of hexagons. For simplicity, the center of the hexagonal patch is taken as the origin of the honeycomb lattice. The periodically placed C_3 axes are also present at the center of the hexagonal patch and at its corners. Note that the C_3 axes at the corners are implied by the existence of the central C_3 axis and the periodic boundary conditions. This basically shows that the electronic spectrum of a (2,6) cage is contained in that of the honeycomb lattice and that it can be selected by applying both periodic and threefold rotational boundary conditions.

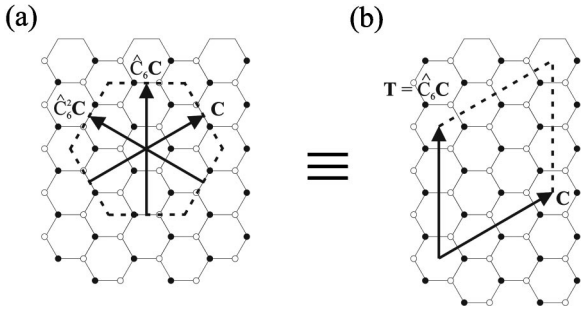

FIG. 3. Patch in the form of (a) a regular hexagon and (b) a rhombus with angles of $\pi/3$ and $2\pi/3$. The vectors $\mathbf{C}$, $\mathbf{T}=\hat{C}_6\mathbf{C}$ and $\hat{C}^2_6\mathbf{C}$ indicate periodic boundary conditions. Both patches define a torus with the same connectivity.

Cutting the hexagonal patch in Fig. 2(c) and gluing the pairs of opposite edges—e.g., applying the periodic but not the rotational boundary conditions—results in a *torus*.[41] Tori have been investigated by Ceulemans *et al.*[35] with the zone-folding method. The torus was obtained by gluing a patch in the form of a general parallelogram, defined by two nonparallel vectors. The Hückel spectrum of this torus can then be derived from that of the honeycomb lattice by selecting the band orbitals of the honeycomb lattice that are periodic along the two nonparallel vectors.

The hexagonal patch in Fig. 3(a) is equivalent to a special type of parallelogram: a rhombus with angles of $\pi/3$ and $2\pi/3$ [Fig. 3(b)]. The two vectors defining this rhombus, $\mathbf{C}$ and $\mathbf{T}$, are totally determined by the indices n_1, n_2

$$\mathbf{C} = (n_1 - n_2)\mathbf{a}_1 + (n_1 + 2n_2)\mathbf{a}_2,$$

$$\mathbf{T} = \hat{C}_6\mathbf{C}. \tag{9}$$

The torus constructed from this rhombus is always a leapfrog. Note that the periodicity over $\mathbf{C}$ and $\hat{C}_6\mathbf{C}$ also implies periodicity over $\hat{C}^2_6\mathbf{C}$, since $\hat{C}^2_6\mathbf{C}=\hat{C}_6\mathbf{C}-\mathbf{C}$. This proves the equivalence of the two patches in Fig. 3.

So applying only the periodic and not the threefold rotational boundary conditions on the honeycomb lattice results

in a torus instead of a (2,6) cage. Hence the spectrum of a (2,6) cage is contained in that of this torus.

Summarizing, we have shown that an octahedrally symmetric (4,6) cage has a part of its Hückel spectrum in common with that of a special kind of torus by using the concept of a (2,6) cage. Since the Hückel eigenvalues and eigenfunctions of any torus are directly retrievable from those of the honeycomb lattice by applying a zone-folding procedure,[35] this part can be found analytically. This will be done in the following section.

IV. ELECTRONIC STRUCTURE OF (2,6) CAGES

A. Electronic structure of the honeycomb lattice

In this section we briefly recall the basic results of the electronic structure of the honeycomb lattice.[42] A unit cell contains two vertices which can be labelled black and white. The basis orbitals that correspond to an irreducible representation $\mathbf{k}$ of the translation group are

$$|\mathbf{k}\rangle_1 = \frac{1}{\sqrt{N}}\sum_{\mathbf{r}_1} \exp(i\mathbf{k}\cdot\mathbf{r}_1)|\mathbf{r}_1\rangle,$$

$$|\mathbf{k}\rangle_2 = \frac{1}{\sqrt{N}}\sum_{\mathbf{r}_2} \exp(i\mathbf{k}\cdot\mathbf{r}_2)|\mathbf{r}_2\rangle. \tag{10}$$

The origin is placed at the center of a hexagon. $\mathbf{r}_1$ denotes the position of a black vertex and $\mathbf{r}_2$ the position of a white vertex

$$\mathbf{r}_1 = m_1\mathbf{a}_1 + m_2\mathbf{a}_2 + \frac{1}{3}(\mathbf{a}_1+\mathbf{a}_2),$$

$$\mathbf{r}_2 = m_1'\mathbf{a}_1 + m_2'\mathbf{a}_2 - \frac{1}{3}(\mathbf{a}_1+\mathbf{a}_2), \tag{11}$$

with m_1, m_2, m_1', m_2' integers. $|\mathbf{r}_j\rangle$ $(j=1,2)$ is a vertex centered at position $\mathbf{r}$. N is the number of unit cells. The Brillouin zone (BZ) takes the shape of a regular hexagon with corners at $\pm(4\pi/3a)\mathbf{e}_y$ and $\pm(2\pi/\sqrt{3}a)\mathbf{e}_x$ $\pm(2\pi/3a)\mathbf{e}_y$ and has basis vectors $\mathbf{b}_1$ and $\mathbf{b}_2$ (Fig. 4)

$$\mathbf{b}_1 = \frac{2\pi}{a}\left(\frac{1}{\sqrt{3}}\mathbf{e}_x + \mathbf{e}_y\right),$$

$$\mathbf{b}_2 = \frac{2\pi}{a}\left(\frac{1}{\sqrt{3}}\mathbf{e}_x - \mathbf{e}_y\right). \tag{12}$$

The interaction matrix element between the basis orbitals in Eq. (10), ${}_1\langle\mathbf{k}|A|\mathbf{k}\rangle_2$, is given by

$$h_{\mathbf{k}} = \exp(i\mathbf{k}(\mathbf{a}_1+\mathbf{a}_2)/3) + \exp(i\mathbf{k}(-2\mathbf{a}_1+\mathbf{a}_2)/3) + \exp(i\mathbf{k}(\mathbf{a}_1-2\mathbf{a}_2)/3). \tag{13}$$

$h_{\mathbf{k}}$ obeys the following relations

$$h_{\hat{C}_6\mathbf{k}} = h_{\mathbf{k}}^* = h_{-\mathbf{k}}, \tag{14}$$

with C_6 a sixfold rotational axis through the origin $\mathbf{\Gamma}=\mathbf{0}$ of the BZ. The eigenfunctions read

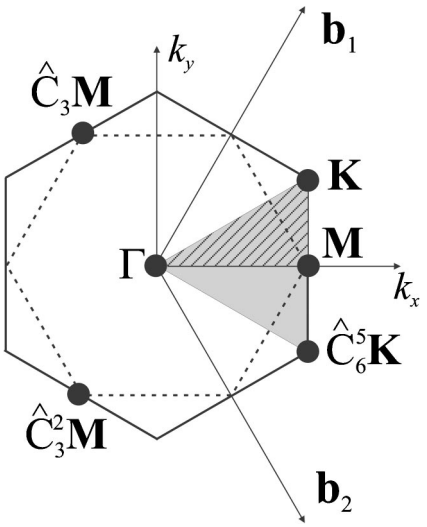

FIG. 4. Brillouin zone of the honeycomb lattice. $\mathbf{b}_1$ and $\mathbf{b}_2$ are the basis vectors. $\mathbf{\Gamma}$, $\mathbf{K}$, $\hat{C}_6^5\mathbf{K}$, $\mathbf{M}$, $\hat{C}_3\mathbf{M}$, and $\hat{C}_3^2\mathbf{M}$ are special symmetry points.

$$|\mathbf{k},\sigma\rangle = \frac{1}{\sqrt{2}}\left(\sigma\sqrt{\frac{h_{\mathbf{k}}}{|h_{\mathbf{k}}|}}|\mathbf{k}\rangle_1 + \sqrt{\frac{h_{\mathbf{k}}^*}{|h_{\mathbf{k}}|}}|\mathbf{k}\rangle_2\right), \tag{15}$$

with $\sigma=1$ for a bonding band orbital and -1 for an antibonding band orbital. The energy belonging to a state $|\mathbf{k},\sigma\rangle$ is equal to

$$\lambda(\mathbf{k},\sigma) = \sigma|h_{\mathbf{k}}| = \sigma\sqrt{1+4\cos\frac{\sqrt{3}k_x a}{2}\cos\frac{k_y a}{2}+4\cos^2\frac{k_y a}{2}},$$

$$\mathbf{k} = k_x\mathbf{e}_x + k_y\mathbf{e}_y. \tag{16}$$

This dispersion relation has C_{6v} symmetry with respect to the principal C_6 axis and the six mirror planes σ_i going through the point $\mathbf{\Gamma}$,

$$\lambda(\hat{C}_6\mathbf{k},\sigma) = \lambda(\mathbf{k},\sigma),$$

$$\lambda(\hat{\sigma}_i\mathbf{k},\sigma) = \lambda(\mathbf{k},\sigma). \tag{17}$$

Special points with respect to the symmetry of the BZ are (Fig. 4) as follows.

(1) The center of the zone $\mathbf{\Gamma}$, with $\lambda(\mathbf{\Gamma},\sigma)=\sigma 3$.

(2) The centers of the edges, corresponding to three distinct states: $\mathbf{M}=(2\pi/\sqrt{3}a)\mathbf{e}_x$, $\hat{C}_3\mathbf{M}$, and $\hat{C}_3^2\mathbf{M}$, with $\lambda(\hat{C}_6^j\mathbf{M},\sigma)=\sigma$.

(3) The corners of the BZ, correspond to two distinct states, $\mathbf{K}=(2\pi/\sqrt{3}a)\mathbf{e}_x+(2\pi/3a)\mathbf{e}_y$ and $\hat{C}_6^5\mathbf{K}$, with $\lambda(\hat{C}_6^j\mathbf{K},\sigma)=0$. At these points, $h_{\mathbf{k}}=0$ hence Eq. (15) cannot be used and σ is not relevant. We use instead as band orbitals $|\mathbf{K}\rangle_1$, $|\mathbf{K}\rangle_2$, $|\hat{C}_6^5\mathbf{K}\rangle_1$, $|\hat{C}_6^5\mathbf{K}\rangle_2$.

In Ref. 36, the band orbitals were distinguished further by their parity with respect to the C_2 axis at the origin. We take this now one step further by symmetrizing the band orbitals with respect to the C_6 axis at the origin:

$$|\mathbf{k},\sigma,j\rangle = \frac{1}{\sqrt{6}}\sum_{t=0}^{5}\hat{C}_6^t\epsilon^{jt}|\mathbf{k},\sigma\rangle, \tag{18}$$

where $\epsilon=\exp(i2\pi/6)$, and $j=0,1,\ldots,5$. The **K** points give rise to the following symmetrized band orbitals

$$|\mathbf{K},j\rangle_{1,2} = \frac{1}{\sqrt{6}}\sum_{t=0}^{5}\hat{C}_6^t\epsilon^{jt}|\mathbf{K}\rangle_{1,2}. \tag{19}$$

The domain of distinct **k** states is $1/6$ of the original BZ and is given by the gray triangle $\mathbf{\Gamma K}(\hat{C}_6^5\mathbf{K})$ in Fig. 4. For each **k** point, one has six band orbitals at $|\lambda_\mathbf{k}|$ (one for each value that j can take), and six band orbitals at $-|\lambda_\mathbf{k}|$. The exceptions are the special symmetry points of the BZ. The distinct possibilities of j given by

$$|\mathbf{\Gamma},\sigma,j\rangle\text{: } \epsilon^j=\sigma,$$

$$|\mathbf{M},\sigma,j\rangle\text{: } \epsilon^{3j}=-\sigma,$$

$$|\mathbf{K},j\rangle_1\text{: } \epsilon^{2j}=\exp(-i2\pi/3),$$

$$|\mathbf{K},j\rangle_2\text{: } \epsilon^{2j}=\exp(i2\pi/3). \tag{20}$$

Use of other symmetry points does not lead to new states.

We can further symmetrize the basis orbitals with respect to the mirror symmetry of the honeycomb lattice (this will only be relevant for cages with O_h symmetry):

$$|\mathbf{k},\sigma,j,\pm,\omega\rangle = \frac{1}{2}[(|\mathbf{k},\sigma,j\rangle \pm |\mathbf{k},\sigma,-j\rangle) + \omega(|\hat{\sigma}_x\mathbf{k},\sigma,j\rangle \pm |\hat{\sigma}_x\mathbf{k},\sigma,-j\rangle)], \tag{21}$$

with $\omega=\pm1$ and

$$j=0,1,2,3 \quad \text{for } |\mathbf{k},\sigma,j,+,\omega\rangle,$$

$$j=1,2 \quad \text{for } |\mathbf{k},\sigma,j,-,\omega\rangle. \tag{22}$$

σ_x is a mirror plane in reciprocal space containing the k_x axis. ω indicates the parity of the orbital with respect to the mirror plane in direct space containing the x axis. The domain of distinct **k** states is $1/12$ of the original BZ and is given by the hatched triangle **ΓKM** in Fig. 4.

B. Electronic structure of the torus

The band orbitals $|\mathbf{k},\sigma\rangle$ of the honeycomb lattice obeying the following periodicity relation,

$$\mathbf{C}\cdot\mathbf{k}=2\pi l_c,$$

$$\mathbf{T}\cdot\mathbf{k}=2\pi l_t, \tag{23}$$

with l_c, l_t integers, are plane waves that coincide with the MOs of the torus defined by **C** and **T**.[35] Only a discrete grid of **k** points fulfills these conditions.

For the special class of tori obeying Eq. (9), this selection is given by

$$k_x = \frac{2\pi}{\sqrt{3}a}\frac{l_c n_1 + l_t n_2}{n_1^2+n_1n_2+n_2^2},$$

TABLE I. Selection of the electronic spectrum when a (2,6) cage is constructed from a torus.

	Multiplicity MOs		
k point	Torus	(2,6) cage	Eigenvalue
$\mathbf{k}\neq\mathbf{\Gamma},\mathbf{M},\mathbf{K}$	6	2	$0<\lvert\lambda\rvert<3$
Γ	1	1	$\lvert\lambda\rvert=3$
M (n_1, n_2 both even)	3	1	$\lvert\lambda\rvert=1$
K	4	0	$\lvert\lambda\rvert=0$

$$k_y = \frac{2\pi}{a}\frac{1}{3}\frac{-l_c(n_1+2n_2)+l_t(2n_1+n_2)}{n_1^2+n_1n_2+n_2^2}. \tag{24}$$

Since the eigenstates of these tori incorporate sixfold symmetry they can be obtained in symmetrized form as $|\mathbf{k},\sigma,j\rangle$ states. Only points within the gray triangle of Fig. 4 must be considered. The special points **Γ**, **K** and **M** on this triangle are represented by the following l_c, l_t numbers:

$$\Gamma=\mathbf{0}\Leftrightarrow l_c=0,\ l_t=0,$$

$$\mathbf{K}\Leftrightarrow l_c=n_1,\ l_t=n_1+n_2,$$

$$\mathbf{M}\Leftrightarrow l_c=n_1+\frac{1}{2}n_2,\ l_t=\frac{1}{2}n_1+n_2. \tag{25}$$

From Eq. (25) it is clear that the **Γ** point and the **K** point are included for any n_1, n_2, but the **M** point is only included when n_1 and n_2 are both even. Most energy levels occur in sextets—one for each value of j—or multiples thereof. The only exceptions are the levels due to the **Γ** point (a singlet at ±3), the **M** point (if included, contributing a triplet at ±1), and the **K** point (a quartet at 0), as is clear from Eq. (20).

The degeneracy can even be higher for tori with $n_2=0$ and $n_2=n_1$, because $|\mathbf{k},\sigma,j,\pm,\omega\rangle$ has the same energy for $\omega=1$ or -1. A **k** point strictly inside the hatched triangle of Fig. 4 corresponds now to a twelvefold degenerate level. **k** points on the special symmetry lines **ΓM**, **ΓK** and **KM** that are no special symmetry points correspond still to sextets.

C. Electronic structure of the (2,6) cage

To obey the boundary conditions for a (2,6) cage, we require in addition to the cyclic boundary conditions that the MO given in Eq. (18) be *totally symmetric* with respect to the central C_3 axis, i.e., $j=0$ or $j=3$. So for each **k** point, the allowed MOs are $|\mathbf{k},\sigma,0\rangle$ and $|\mathbf{k},\sigma,3\rangle$. This reduces the number of allowed MOs to $1/3$ compared to those of the torus. The selection of the electronic spectrum when passing from the torus to the (2,6) cage is given in Table I. Most **k** points of the (2,6) cage will give rise to doublets, but there are a few exceptions. At $\lambda=\pm3$ there is always a nondegenerate energy level due to the **Γ** point. For n_1, n_2 both even, there exists an odd-degenerate level at $\lambda=\pm1$ because the **M** point contributes one single MO at this energy, while other **k** points can possibly contribute to this energy, but only with

an even number of MOs. All **k** points on straight lines between neighboring **M** points and their antipodes (the dashed line in Fig. 4) belong to the eigenvalue $\lambda = \pm 1$. It is sufficient to consider the points inside the gray triangle of Fig. 4, or equivalently all points on the dashed line between **M** and $\hat{C}_6\mathbf{M}$. The necessary and sufficient condition for the (l_c, l_t) pair to generate a MO with eigenvalue ±1 and that is no **M** point is

$$3(n_1^2 + n_1 n_2 + n_2^2) = 2[l_c(n_1 - n_2) + l_t(n_1 + 2n_2)],$$

$$\frac{1}{2}(n_1 - n_2) < l_c < n_1 + \frac{1}{2}n_2,$$

$$\frac{1}{2}n_1 + n_2 < l_t < n_1 + \frac{1}{2}n_2. \tag{26}$$

It is clear that both n_1 and n_2 must be even, otherwise no levels at $\lambda = \pm 1$ will be present. For the special cases $n_2 = 0$ and $n_2 = n_1$ one has

$$n_2 = 0 \Rightarrow (l_c, l_t) = \left(l_c, \frac{3}{2}n_1 - l_c\right), \quad \text{with } \frac{1}{2}n_1 < l_c < n_1,$$

$$n_2 = n_1 \Rightarrow (l_c, l_t) = \left(l_c, \frac{3}{2}n_1\right), \quad \text{with } 0 < l_c < \frac{3}{2}n_1. \tag{27}$$

Adding the single contribution from the **M** point, the degeneracies at $\lambda = \pm 1$ are for n_1 even

$$n_2 = 0 \Rightarrow 1 + 2\left(\frac{1}{2}n_1 - 1\right) = n_1 - 1,$$

$$n_2 = n_1 \Rightarrow 1 + 2\left(\frac{3}{2}n_1 - 1\right) = 3n_1 - 1. \tag{28}$$

As for the **K** points, since Eq. (20) shows that they cannot be totally symmetric with respect to the C_3-axis, the energy level $|\lambda| = 0$ is never included. In other words, octahedrally symmetric (4,6) cages will never have a nonbonding MO of the $A+E$ group.

For $n_2 = 0$ and $n_2 = n_1$, all **k** points strictly inside the hatched triangle of Fig. 4 correspond to quartets. The points on the borders of this triangle that are no special symmetry points, correspond to doublets; on the line **ΓM** ω can only be unity, on the line **ΓK** $\epsilon^j \times \omega$ must be equal to σ and on the line **KM** $\epsilon^j \times \omega$ must be equal to $-\sigma$.

Summarizing, by combining Eqs. (16), (18), and (24), the eigenvalues and eigenvectors of A_1, A_2, and E symmetry of octahedrally symmetric (4,6) cages can be obtained. In the following section we will show how to make a distinction between these three representations.

V. IRREDUCIBLE SYMMETRY REPRESENTATIONS

Simple counting of orbits (sets of equivalent positions) allows a complete breakdown of the eigenvector symmetries in all O and O_h cages. There are five cases.

(1) Nonleapfrog cage, O symmetry

$$\Gamma_\sigma = \frac{1}{3}\left(\frac{1}{8}v_{(4,6)} + 2\right)A_1 + \frac{1}{3}\left(\frac{1}{8}v_{(4,6)} + 2\right)A_2 + \frac{2}{3}\left(\frac{v_{(4,6)}}{8} - 1\right)E + \frac{v_{(4,6)}}{8}T_1 + \frac{v_{(4,6)}}{8}T_2. \tag{29}$$

(2) Leapfrog cage, O symmetry

$$\Gamma_\sigma = \frac{v_{(4,6)}}{24}A_1 + \frac{v_{(4,6)}}{24}A_2 + \frac{v_{(4,6)}}{12}E + \frac{v_{(4,6)}}{8}T_1 + \frac{v_{(4,6)}}{8}T_2. \tag{30}$$

(3) Nonleapfrog zigzag cage, O_h symmetry

$$\Gamma_\sigma = \frac{(n_1+1)(n_1+2)}{6}A_{1g} + \frac{(n_1-1)(n_1-2)}{6}A_{2g} + \frac{(n_1+1)(n_1-1)}{3}E_g + \frac{n_1(n_1-1)}{2}T_{1g} + \frac{n_1(n_1+1)}{2}T_{2g} + \frac{(n_1-1)(n_1-2)}{6}A_{1u} + \frac{(n_1+1)(n_1+2)}{6}A_{2u} + \frac{(n_1+1)(n_1-1)}{3}E_u + \frac{n_1(n_1+1)}{2}T_{1u} + \frac{n_1(n_1-1)}{2}T_{2u}. \tag{31}$$

(4) Leapfrog zigzag cage, O_h symmetry

$$\Gamma_\sigma = \frac{n_1(n_1+3)}{6}A_{1g} + \frac{n_1(n_1-3)}{6}A_{2g} + \frac{n_1^2}{3}E_g + \frac{n_1(n_1-1)}{2}T_{1g} + \frac{n_1(n_1+1)}{2}T_{2g} + \frac{n_1(n_1-3)}{6}A_{1u} + \frac{n_1(n_1+3)}{6}A_{2u} + \frac{n_1^2}{3}E_u + \frac{n_1(n_1+1)}{2}T_{1u} + \frac{n_1(n_1-1)}{2}T_{2u}. \tag{32}$$

(5) Leapfrog armchair cage, O_h symmetry,

$$\Gamma_\sigma = \frac{n_1(n_1+1)}{2}A_{1g} + \frac{n_1(n_1+1)}{2}A_{2g} + n_1(n_1+1)E_g + \frac{n_1(3n_1-1)}{2}T_{1g} + \frac{n_1(3n_1-1)}{2}T_{2g} + \frac{n_1(n_1-1)}{2}A_{1u} + \frac{n_1(n_1-1)}{2}A_{2u} + n_1(n_1-1)E_u + \frac{n_1(3n_1+1)}{2}T_{1u} + \frac{n_1(3n_1+1)}{2}T_{2u}. \tag{33}$$

Because the (4,6) cage is an alternant, its spectrum is bipartite: for each bonding MO at $+|\lambda|$ there exists an antibonding MO at $-|\lambda|$ with the same coefficient on white vertices but an opposite value on black vertices.[43,44] This implies an opposite behavior of both MOs with respect to the C_4 axes which interchange black and white vertices. So the following relationships between the symmetries of the two MOs at opposite energy exist:

$$A_1 \leftrightarrow A_2,$$

$$E \leftrightarrow E,$$

$$T_1 \leftrightarrow T_2. \tag{34}$$

When the point group is O_h, we have also the additional relation

$$\text{zigzag cage: } \Gamma_g \leftrightarrow \Gamma_u', \tag{35}$$

$$\text{armchair cage: } \Gamma_g \leftrightarrow \Gamma_g', \tag{36}$$

with Γ and Γ' symmetry labels of O, obeying the relationship (34).

The energy levels of the $A+E$ group can be obtained analytically. Counting degeneracies explicitly, they cover $1/4$ of the spectrum of the (4,6) cage. Using Eqs. (29) or (30) and counting symmetry—but not accidentally—degenerate eigenvalues as one, they correspond to $2/5$ of the distinct eigenvalues of a leapfrog (4,6) cage, and $[2(v_{(4,6)}/8)+1]/[5(v_{(4,6)}/8)+1]$ of a nonleapfrog.

To determine whether a given MO of the (2,6) cage corresponds to an A_1, A_2 or E representation of the (4,6) cage, we first note that most MOs are doubly degenerate, i.e., one MO for $j=0$ and one for $j=3$. A MO of the (2,6) cage with $j=0$ corresponds to a MO of the folded (4,6) cage that is symmetric with respect to all C_4 axes of the (4,6) cage, while a MO of the (2,6) cage with $j=3$ corresponds to a MO of the folded (4,6) cage that is antisymmetric with respect to all C_4 axes of the (4,6) cage. Hence all these doubly degenerate levels have $\chi(C_4)=0$. From the octahedral character one obtains

$$\chi^{A_1}(C_4) = 1,$$

$$\chi^{A_2}(C_4) = -1,$$

$$\chi^{E}(C_4) = 0, \tag{37}$$

which implies that the doublets must have either A_1+A_2 or E symmetry.

These two possibilities can be distinguished by their character under any threefold rotation axis in O:

$$\chi^{A_1+A_2}(C_3) = 2,$$

$$\chi^{E}(C_3) = -1. \tag{38}$$

These C_3 axes of the (4,6) cage run through the triangle midpoints of the master octahedron. They run through an atom in the case of a nonleapfrog cage and through the center of a hexagon in the case of a leapfrog cage. On the unfolded hexagonal patch of the torus on the honeycomb lattice they can be identified with the threefold axes at positions $\hat{C}_6^j(\frac{1}{3}\mathbf{C})$, $j=0,1,\ldots,5$. Figure 5(a) gives two examples—corresponding to nonleapfrog (left) and leapfrog (right) cages—where these threefold axes are presented by gray triangles. Take a MO of the honeycomb lattice that obeys the periodicity conditions of the hexagonal patch defined by **C** [big black hexagon in Fig. 5(a)] and that is totally symmetric with respect to the threefold axes at the center and the corners of this patch [black triangles in Fig. 5(a)]. When this MO is also totally symmetric with respect to the threefold axes at the corners of the hexagonal patch defined by **N** [gray triangles in Fig. 5(a)], it will automatically obey the periodicity conditions of this smaller hexagonal patch [small gray hexagon in Fig. 5(a)]. So MOs that are A_1 and A_2 representations in the (4,6) cage, correspond to MOs of the honeycomb lattice that are periodic over **N** and $\hat{C}_6\mathbf{N}$. Each hexagonal patch defines a torus, and the bigger one, defined by $\mathbf{C}=(n_1-n_2)\mathbf{a}_1+(n_1+2n_2)\mathbf{a}_2$, is the leapfrog of the smaller one, defined by $\mathbf{N}=n_1\mathbf{a}_1+n_2\mathbf{a}_2$. The periodic boundary conditions of the small hexagonal patch defines the following grid of **k** points:

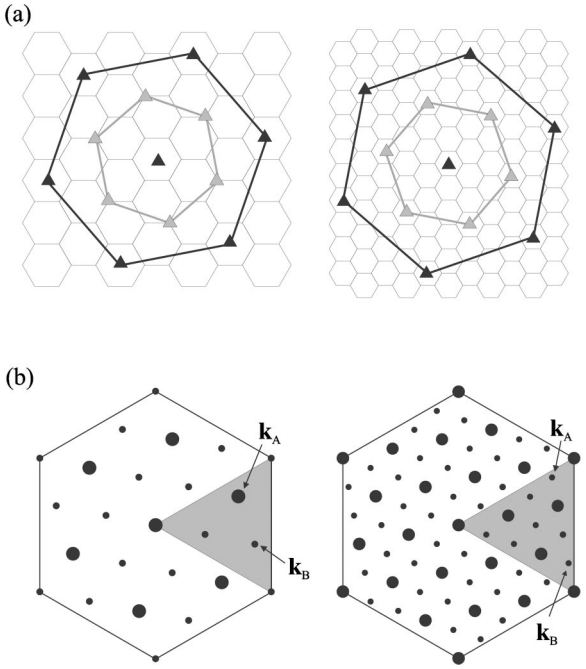

FIG. 5. Two examples on how to distinguish the A_1 and A_2 representations of a (4,6) cage from the E representations. The left part treats a nonleapfrog (4,6) cage with indices $n_1=2$, $n_2=1$ and the right part a leapfrog (4,6) cage with indices $n_1=4$, $n_2=1$. (a) The honeycomb lattice. As we have seen before, MOs that obey the periodicity conditions defined by the larger black hexagonal patch and that are totally symmetric with respect to the central threefold axis, correspond to MOs of the $A+E$ group of the (4,6) cage. The smaller gray hexagonal patch defines a torus that is the parent of the torus defined by the larger black hexagonal patch. MOs that obey the periodicity conditions defined by this smaller patch correspond to the A_1 and A_2 representations. (b) **k** points in the Brillouin zone that obey the periodicity conditions of the larger black hexagonal patch in (a). The heavy dots obey the periodicity conditions of the smaller gray hexagonal patch and hence correspond to A_1 and A_2 representations, the small dots to E representations. $\mathbf{k}_A$ and $\mathbf{k}_B$ correspond to the MOs with the two energies closest to zero. They correspond respectively to one E representation and one A_1+A_2 couple in the case of the nonleapfrog cage, and to two E representations in the case of the leapfrog cage.

$$k_x = \frac{2\pi}{\sqrt{3}a}\frac{l_c'(2n_1+n_2)+l_t'(n_2-n_1)}{n_1^2+n_1n_2+n_2^2},$$

TABLE II. Symmetry labels of O_h (4,6) cages for MOs resulting from **k** points on the borders of the triangle **ΓKM**. Symbols like]**ΓM**[denote all **k** points on the line between **Γ** and **M**, the **Γ** and **M** end points not included.

k	σ	Zigzag	Armchair
Γ	1	A_{1g}	A_{1g}
Γ	−1	A_{2u}	A_{2g}
M	1	A_{2u}	A_{2g}
M	−1	A_{1g}	A_{1g}
]**ΓM**[	1 or −1	$A_{1g}+A_{2u}$	$A_{1g}+A_{2g}$ or E_g
]**ΓK**[	1	$A_{1g}+A_{2g}$ or E_g	$A_{1g}+A_{2u}$
]**ΓK**[	−1	$A_{1u}+A_{2u}$ or E_u	$A_{1u}+A_{2g}$
]**KM**[	1	$A_{1u}+A_{2u}$ or E_u	$A_{1u}+A_{2g}$
]**KM**[	−1	$A_{1g}+A_{2g}$ or E_g	$A_{1g}+A_{2u}$

$$k_y = \frac{2\pi}{a}\frac{-l_c' n_2 + l_t'(n_1+n_2)}{n_1^2+n_1 n_2+n_2^2}, \tag{39}$$

with l_c', l_t' any integer. This grid is a subspace of the finer grid defined by Eq. (24). The selection rule for states to be a A_1+A_2 couple is

$$l_c + l_t = 3l_c',$$

$$-l_c + 2l_t = 3l_t'. \tag{40}$$

About one third of the states is selected in this way, in accordance with Eqs. (29) and (30). An example is shown in Fig. 5(b). For each A_1+A_2 couple, the MO with $j=0$ corresponds to the A_1 representation and the MO with $j=3$ corresponds to the A_2 representation.

The **Γ** point and, if allowed, the **M** point, always obey Eq. (40). Since they correspond to only one MO each at one energy, they will give rise to *either* A_1 or A_2 representations. Inspection of the symmetry parameter j and the index σ in Eq. (20) reveals that the totally bonding MO at the **Γ** point will always be of A_1 symmetry and the totally antibonding MO always of A_2 symmetry. If present, the bonding MO at the **M** point is always of A_2 symmetry and the antibonding MO of A_1 symmetry.

For zigzag cages with n_1 even, one has—apart from the MO due to the **M** point—(n_1-2) MOs at energies ±1 [Eq. (28)]. Combining Eqs. (27) and (40) it is clear that they correspond to $(n_1/2-1)$ doublets of A_1+A_2 symmetry. In other words, this class of cages has a very high density of A states at this energy.

The zigzag and armchair cages have O_h symmetry. Their MOs are given by $|\mathbf{k},\sigma=\pm1,j=0 \text{ or } 3,+,\omega=\pm1\rangle$. Each **k** point that is strictly inside the triangle **ΓKM** corresponds to an accidentally degenerate $A_{1g}+A_{2g}+A_{1u}+A_{2u}$ quartet or to an E_g+E_u quartet for both types of cages. The representation of a MO of a zigzag cage (armchair cage) is gerade when $\epsilon^j\omega$ (ω) is equal to 1 and ungerade when $\epsilon^j\omega$ (ω) is equal to −1. In Table II an overview is given of the possible symmetry representations of **k** points on the borders of the triangle **ΓKM** for the zigzag and armchair cages.

Note that Eq. (40) is always fulfilled for points on the border **ΓM** for zigzag cages and for points on the borders **ΓK** or **KM** for armchair cages.

VI. ENERGY AND SYMMETRY OF FRONTIER ORBITALS OF THE $A+E$ GROUP

In this section we will deduce the value and the symmetry of MOs of the $A+E$ group that are closest to $\lambda=0$.

In the grid of allowed **k** states [Eq. (24)], the six points closest to a **K** point will correspond to the energies closest to zero. Only two of these points are within the gray zone in Fig. 4 and will give rise to nonidentical MOs in the (4,6) cage. Their position is given by

$$l_c = n_1, \quad l_t = n_1+n_2-1, \quad \text{for } \mathbf{k}_A, \text{ the point near } \mathbf{K},$$

$$l_c = n_2+n_1-1, \quad l_t = n_2, \quad \text{for } \mathbf{k}_B, \text{ the point near } \hat{C}_6^5\mathbf{K}. \tag{41}$$

Examples are shown in Fig. 5(b). The energy corresponding to these two points can be found by combining Eqs. (16), (24), and (41). However, the expression is easier to interpret if we make first a Taylor expansion of $\lambda(\mathbf{k},\sigma)$ in the points **K** and $\hat{C}_6^5\mathbf{K}$:

$$\lambda^2(\mathbf{K}+\Delta\mathbf{k},\sigma) \approx \frac{3}{4}(\Delta k_x^2+\Delta k_y^2)a^2 + \frac{\sqrt{3}}{8}\Delta k_y(\Delta k_y^2-3\Delta k_x^2)a^3, \tag{42}$$

$$\lambda^2(\hat{C}_6^5\mathbf{K}+\Delta\mathbf{k},\sigma) \approx \frac{3}{4}(\Delta k_x^2+\Delta k_y^2)a^2 - \frac{\sqrt{3}}{8}\Delta k_y(\Delta k_y^2-3\Delta k_x^2)a^3. \tag{43}$$

For points given in (41), $\Delta\mathbf{k}$ is equal to

$$\Delta\mathbf{k} = -\frac{2\pi}{\sqrt{3}a}\frac{n_2}{n_1^2+n_1n_2+n_2^2}\mathbf{e}_x - \frac{2\pi}{3a}\frac{2n_1+n_2}{n_1^2+n_1n_2+n_2^2}\mathbf{e}_y, \text{ for } \mathbf{k}_A,$$

$$\Delta\mathbf{k} = -\frac{2\pi}{\sqrt{3}a}\frac{n_1}{n_1^2+n_1n_2+n_2^2}\mathbf{e}_x + \frac{2\pi}{3a}\frac{n_1+2n_2}{n_1^2+n_1n_2+n_2^2}\mathbf{e}_y, \text{ for } \mathbf{k}_B. \tag{44}$$

We find for λ^2

$$\begin{aligned}\lambda^2(\mathbf{k}_A,\sigma) &\approx \frac{4\pi^2}{3}\frac{1}{n_1^2+n_1n_2+n_2^2} \\ &\quad\times\left(1-\frac{\pi}{3\sqrt{3}}\frac{(2n_1+n_2)(n_1+2n_2)(n_1-n_2)}{(n_1^2+n_1n_2+n_2^2)^2}\right) \\ &= \frac{4\pi^2a^2}{3d^2}\left(1-\frac{2\pi a}{3\sqrt{3}d}\sin 3\theta\right),\end{aligned} \tag{45}$$

$$\lambda^2(\mathbf{k}_B,\sigma) \approx \frac{4\pi^2}{3}\frac{1}{n_1^2+n_1n_2+n_2^2} \times\left(1+\frac{\pi}{3\sqrt{3}}\frac{(n_1+2n_2)(2n_1+n_2)(n_1-n_2)}{(n_1^2+n_1n_2+n_2^2)^2}\right) = \frac{4\pi^2a^2}{3d^2}\left(1+\frac{2\pi a}{3\sqrt{3}d}\sin 3\theta\right), \quad (46)$$

where we have used the geometrical parameters d—the distance between the centers of two nearest-neighbor squares and proportional to the number of atoms—and θ, the chiral angle between **N** and the x axis:

$$d = |\mathbf{N}| = \sqrt{n_1^2+n_1n_2+n_2^2}\,a, \quad (47)$$

$$\tan\theta = \frac{1}{\sqrt{3}}\frac{n_1-n_2}{n_1+n_2}. \quad (48)$$

Note that the dependence of $\lambda(\mathbf{k}_{A,B},\sigma)$ on the chiral angle θ is only a higher order effect. By definition (48), $\theta=0$ for armchair cages and $\theta=\pi/6$ for zigzag cages. Thus we find for the energy of the two levels closest to energy zero that belong to the $A+E$ group

$$\lambda(\mathbf{k}_{A,B},\sigma) \approx \sigma\frac{2\pi a}{\sqrt{3}d}\sqrt{1\pm\frac{2\pi a}{3\sqrt{3}d}\sin 3\theta}, \quad (49)$$

where the $-$ sign refers to $\mathbf{k}_A$ and the $+$ sign to $\mathbf{k}_B$. We note that $|\lambda_{\mathbf{k}_A}| \leqslant |\lambda_{\mathbf{k}_B}|$ if we confine ourselves to the sufficient domain $n_1 \geqslant n_2 \geqslant 0$ or equivalently $\pi/6 \geqslant \theta \geqslant 0$. The splitting between the two energies is equal to

$$|\lambda(\mathbf{k}_B,\sigma)| - |\lambda(\mathbf{k}_A,\sigma)| \approx \frac{2\pi a}{\sqrt{3}d}\left(\sqrt{1+\frac{2\pi a}{3\sqrt{3}d}\sin 3\theta} - \sqrt{1-\frac{2\pi a}{3\sqrt{3}d}\sin 3\theta}\right) \approx \frac{4\pi^2a^2}{9d^2}\sin 3\theta. \quad (50)$$

A fourfold degenerate level is obtained for armchair cages while the splitting is maximal for zigzag cages.

Apart from the energy of the MO, also its shape is important. Consider the atomic orbital coefficient at position $\mathbf{r}_1=\frac{1}{3}(\mathbf{a}_1+\mathbf{a}_2)$. This atom is part of a square in the folded (4,6) cage. From Eq. (18), one finds that this coefficient is equal to

$$\left\langle \mathbf{r}_1=\frac{1}{3}(\mathbf{a}_1+\mathbf{a}_2)|\mathbf{k},\sigma,j\right\rangle = \frac{1}{\sqrt{12N}}\left(\sigma\sqrt{\frac{h_{\mathbf{k}}}{|h_{\mathbf{k}}|}}h_{\mathbf{k}} + \epsilon^j\sqrt{\frac{h_{\mathbf{k}}^*}{|h_{\mathbf{k}}|}}h_{\mathbf{k}}^*\right). \quad (51)$$

Like $\lambda(\mathbf{k},\sigma)$, $h_{\mathbf{k}}$ goes to zero when $\mathbf{k}$ approaches $\mathbf{K}$:

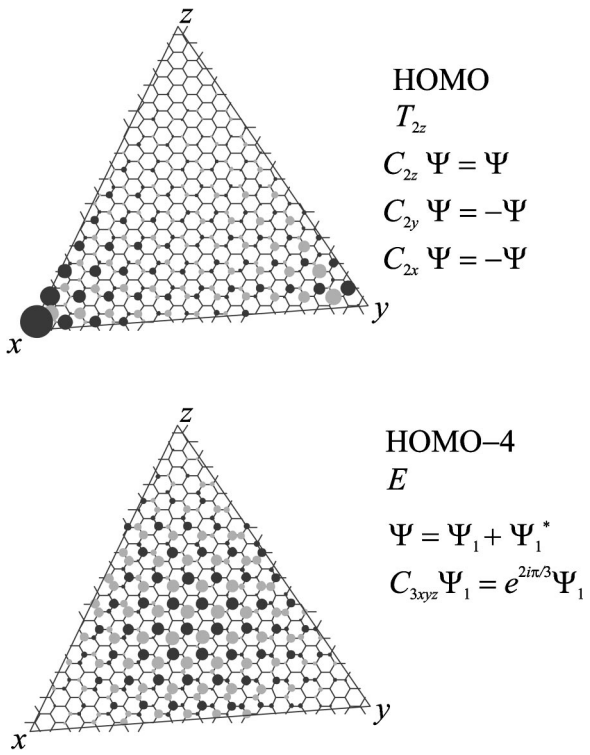

FIG. 6. Plot of the highest bonding MO of the T group and the highest bonding MO of the $A+E$ group of the (4,6) cage $n_1=13$, $n_2=10$. Only one master triangle of the cage is shown. x, y, z denote the positions of the three C_4 axes. The precise conditions used to extract the shown MO are also given. Top: this MO is the HOMO and has T_2 symmetry. The T_{2z} component is shown. The MO is enhanced around the squares going through the x and y axes, but is vanishing around the squares going through the z axis. Bottom: this MO is the HOMO-4 and has E symmetry. It is vanishing around all the squares.

$$h_{\mathbf{K}+\Delta\mathbf{k}} \approx \frac{3}{4}\left(1+\frac{i}{\sqrt{3}}\right)(-\Delta k_x + i\Delta k_y)a, \quad \to 0 \quad \text{for } \Delta\mathbf{k}\to 0. \quad (52)$$

It follows that MOs of the $A+E$ group close to energy zero have a very low value around the squares, with the MOs corresponding to $\mathbf{k}_A$ and $\mathbf{k}_B$ as the most extreme cases. An example is shown in Fig. 6.

The symmetries of the energy levels $\lambda(\mathbf{k}_B,\sigma)$ and $\lambda(\mathbf{k}_A,\sigma)$ can be found by confronting the expression for l_c, l_t with the selection rule (40).

For the leapfrog (4,6) cages both energy levels correspond to E representations, while for the nonleapfrogs type 1 (type 2) the energy level closest to energy zero corresponds to an E representation (A_1+A_2 couple) and the next level to an A_1+A_2 couple (E representation). Exceptions to this rule are the smallest cages $n_1=1$, $n_2=0$, $n_1=1$, $n_2=1$ and $n_1=2$, $n_2=0$ because $\mathbf{k}_A$ and $\mathbf{k}_B$ are symmetry related and/or correspond to the special symmetry points $\mathbf{\Gamma}$ or $\mathbf{M}$.

$\mathbf{k}_A \in]\mathbf{KM}]$ and $\sigma_x\mathbf{k}_B \in [\mathbf{\Gamma K}[$ for zigzag cages. Hence the bonding (antibonding) energy level of the $A+E$ group closest to energy zero is ungerade (gerade) while the next bonding

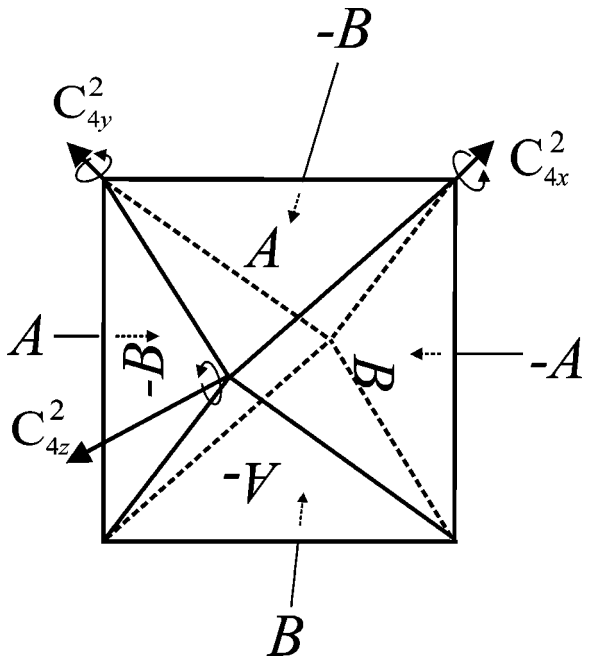

FIG. 7. An octahedron with a A/B pattern inscribed that is even under action of the C^2_{4y} axis but odd under action of the C^2_{4x} and C^2_{4z} axis.

(antibonding) energy level is gerade (ungerade). Armchair cages have one fourfold degenerate level with symmetry labels E_g+E_u, due to the fact that $\mathbf{k}_A$ and $\mathbf{k}_B$ are symmetry related.

Note that there is no important difference between leapfrog and nonleapfrog (4,6) cages with respect to the position of the energy levels of the $A+E$ group close to $\lambda=0$. This is in contrast with the very different electronic structure for leapfrogs and non-leapfrogs close to $\lambda=0$ in the case of fullerenes,[39] (3,6) cages,[36] nanotubes,[34] and tori.[35] On the other hand, as we will see in the next section, the position of energy levels of the T group close to $\lambda=0$ are clearly different for leapfrog and nonleapfrog (4,6) cages.

VII. MOs OF THE *T* GROUP: NUMERICAL HÜCKEL CALCULATIONS

A general treatment of the MOs of the T group poses a problem that was not met for MOs of the $A+E$ group. Take for example the y component of a MO of the T group: the MO should be even under action of the C^2_{4y} axis but odd under action of the C^2_{4x} and C^2_{4z} axis (Fig. 7). Let us label two adjacent triangles of the master octahedron A and B, respectively; the other triangles are labeled by action of the 3 C^2_4 axes. The triangle $\pm A$ has $\mp B$ as two of its neighbors and $\pm B$ as the third. A similar condition applies for the triangle $\pm B$. It is not possible to place a periodic pattern on the plane, using as tiles the triangles $\pm A$ and $\pm B$, where each triangle has the same neighbors as for the octahedron. So the zone-folding procedure applied previously to MOs of the $A+E$ group cannot be used for the T group. However, the frontier orbitals of the octahedral (4,6) cages will always be of T symmetry, as shown in Ref. 45. We have therefore performed numerical Hückel calculations on all octahedral (4,6) cages with $n_2 \leqslant n_1 \leqslant 29$.

A. Position of the HOMO

Let us denote the smallest positive eigenvalue of a graph as λ_{HOMO}. The HOMO-LUMO gap is then equal to

$$E_g = 2|\beta_{\mathrm{CC}}|\lambda_{\mathrm{HOMO}} \quad \text{for carbon cages,} \tag{53}$$

$$E_g = 2\sqrt{\Delta^2 + \beta^2_{\mathrm{BN}}\lambda^2_{\mathrm{HOMO}}} \quad \text{for BN cages.} \tag{54}$$

In Fig. 8, $\lambda^2_{\mathrm{HOMO}}$ of the (4,6) cages is plotted versus $1/(n_1^2+n_2^2+n_1n_2)=1/d^2$ for different classes of cages. It is immediately clear that λ_{HOMO} of nonleapfrog cages is smaller than that of leapfrog cages with a similar size, as already noted in Ref. 21. A detailed analysis of the data leads to the following conclusions.

(1) *Leapfrog cages*: the data points (triangles in Fig. 8) follow more or less a smooth line which means that λ_{HOMO} is determined mostly by d and only slightly by θ. λ_{HOMO} is

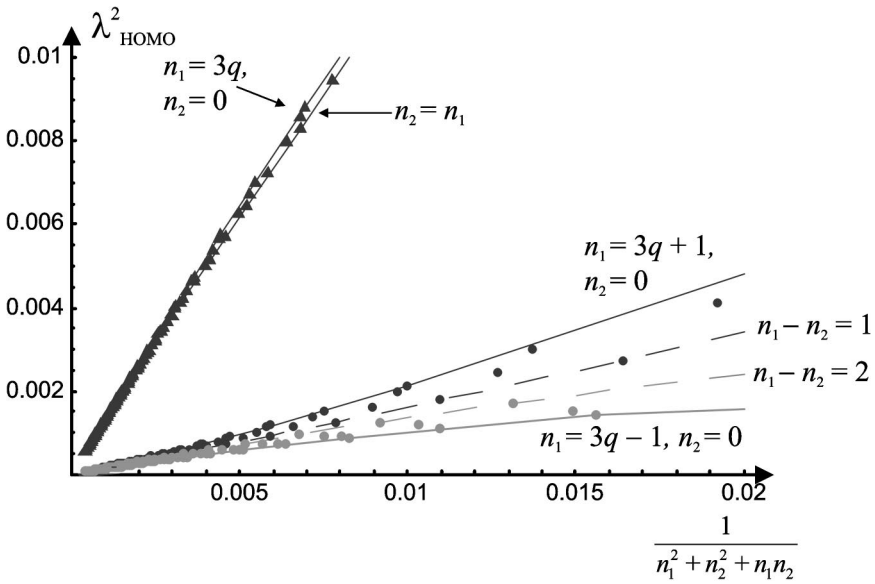

FIG. 8. Data plot of λ_{HOMO} versus $1/(n_1^2+n_2^2+n_1n_2)$ for leapfrog cages (triangles), nonleapfrog cages type 1 (black points) and type 2 (gray points). Leapfrog cages, upper line: zigzag leapfrog cages. Leapfrog cages, lower line: armchair cages. Nonleapfrog cages, black line: zigzag nonleapfrog cages type 1. Nonleapfrog cages, gray line: zigzag nonleapfrog cages type 2. Black dashed line: cages corresponding to $n_1-n_2=1$. Gray dashed line: cages corresponding to $n_1-n_2=2$.

maximal for zigzag cages and minimal for armchair cages. The distribution of the data points in Fig. 8 suggests that $\lambda^2_{\mathrm{HOMO}}$ can be approximated in the following way:

$$\lambda^2_{\mathrm{HOMO}}(d,\theta) \approx \frac{b_0(\theta)}{d^2} + \frac{b_1(\theta)}{d^3} + \frac{b_2(\theta)}{d^4} + \frac{b_3(\theta)}{d^5} + \cdots . \tag{55}$$

Equation (55) has the same formal form as the Taylor expansion used in Eq. (45) to obtain the minimal eigenvalue of the $A+E$ group, but the coefficients $b_0, b_1, \ldots$ are unknown. Fitting $\lambda^2_{\mathrm{HOMO}}$ to Eq. (55) using groups of cages with varying d but fixed θ gives for b_0

$$b_0(\theta) = b_0 \approx 1.368, \tag{56}$$

i.e., the lowest order term in Eq. (55) is independent of θ. $b_1(\theta)$ is negative and varies between

$$b_1(0) \approx -1.881 < b_1(0 < \theta < \pi/6) < b_1(\pi/6) \approx -1.174. \tag{57}$$

(2) *Nonleapfrog cages*: the points are more widely scattered. λ_{HOMO} is higher for nonleapfrogs of type 1 (black points in Fig. 8) than for cages of type 2 (gray points in Fig. 8). Zigzag nonleapfrog cages of type 1 (type 2) have a maximal (minimal) λ_{HOMO}. λ_{HOMO} is more or less in the middle of these two extremes for cages with a minimal θ ($n_1-n_2=1$ or 2). Fitting $\lambda^2_{\mathrm{HOMO}}$ to Eq. (55) for nonleapfrog cages of one type and with fixed θ gives the following result for b_0

$$b_0(\theta) = b_0 \approx 0.153, \tag{58}$$

so again the lowest order term is independent of θ. b_1 is positive for nonleapfrog cages of type one and negative for nonleapfrog cages of type two. The absolute value varies between

$$|b_1(\theta \to 0)| \approx 0 < |b_1(0 < \theta < \pi/6)| < |b_1(\pi/6)| \approx 0.556. \tag{59}$$

B. Shape of the frontier orbitals

From Fig. 6 one can see that the MOs of the T group close to energy zero are enhanced in the neighborhood of some of the squares. More precisely, the T_z component is vanishing around the squares going through the z axis but enhanced around the squares going through the x and y axes. This behavior holds both for leapfrog and nonleapfrog cages and is clearly different to that of the MOs of the $A+E$ group close to energy zero (vide supra).

C. Symmetry of the frontier orbitals

Finally we give an overview of the symmetries of the bonding MOs close to energy zero.

(1) *Leapfrog cages*: The HOMO and HOMO−1 of leapfrog cages are both of T_2 symmetry. The HOMO is of T_{2u} and the HOMO−1 of T_{2g} symmetry for armchair cages, while the reverse is true for zigzag cages. There can be zero, one or two MOs of T_1 symmetry between the HOMO−1 and the first MO of the $A+E$ group.

(2) *Nonleapfrog cages*: the HOMO is always of T_1 symmetry (T_{1u} for zigzag nonleapfrogs type 1 and T_{1g} for zigzag nonleapfrogs type 2). Excluding the smallest cages $n_1=1, n_2=0$ and $n_1=2, n_2=0$, the HOMO−1 and the HOMO−2 are of T_1 and T_2 symmetry respectively (T_{1g}, T_{2u} for zigzag nonleapfrogs type 1 and T_{1u}, T_{2g} for zigzag nonleapfrogs type 2). The next level is of the $A+E$ group.

By using relation Eq. (34), one can find the rules for the lowest antibonding MOs. The rules for identifying HOMO −1, HOMO, LUMO and LUMO+1 in the case of leapfrog cages, and for identifying HOMO and LUMO in the case of nonleapfrog cages, are rigorously proven in Ref. 45 using group theory.

So it is clear that leapfrog and non-leapfrog cages are different not only with respect to the position of the frontier orbitals, but also with respect to their symmetries. The origin of this difference is clarified in Ref. 45.

VIII. COMPARISON WITH QUANTUM CHEMICAL CALCULATIONS

In order to test the validity of the simple tight-binding approximation, we have performed a standard density-functional theory (DFT) calculation on several octahedral (4,6) cages. The B3LYP functional was used, in combination with the split-valence basis sets from Schäfer *et al.*[46] extended with a polarization function with exponent 0.80. This DFT calculation was performed with the Turbomole code.[47]

The smallest leapfrog octahedral (4,6) cage is the truncated octahedron C_{24} ($n_1=1, n_2=1$). This cage was optimized under O_h symmetry constraints. The total binding energy per carbon atom is 6.22 eV. The symmetry of the energy levels from HOMO−1 to LUMO is the same as those from the Hückel calculations. The symmetry of both the highest bonding and lowest antibonding MO of the $A+E$ group is E_g, as predicted by the Hückel model.

Next we have investigated the O cage C_{56} ($n_1=2, n_2=1$), which is a nonleapfrog. In this case the binding energy per carbon atom is higher, 6.83 eV, which reflects that the strain in this larger cage is relaxed as compared to C_{24}. The symmetries of HOMO and LUMO are the same as those obtained from the Hückel calculations. The symmetry of both the highest bonding and lowest antibonding MO of the $A+E$ group is E, as predicted for a nonleapfrog cage type 1.

Finally we have also investigated the C_{72} zigzag leapfrog cage ($n_1=3, n_2=0$) and its BN counterpart. The binding energy per carbon atom is again higher, 6.93 eV per carbon atom. Comparing DFT with Hückel, the symmetry of the energy levels agrees from HOMO−6 to LUMO for the carbon cage (see Table III). The LUMO+1 and LUMO+2 calculated with DFT have switched position compared to the Hückel results, but are still very close in energy. Fitting the DFT and Hückel results by Eq. (2) provides us with the fitting parameters $\alpha_C=-4.58$ eV and $\beta_{CC}=-2.87$ eV and a R^2 value of 0.96. The agreement is even better for the BN cage; there is a symmetry match of the energy levels from HOMO−6 to LUMO+2. Fitting the DFT and Hückel results by Eq. (4) gives the following parameters: $\alpha_{BN}=-3.77$ eV, $\beta_{BN}=-2.67$ eV and $|\Delta|=2.47$ eV.

TABLE III. Orbital energies and symmetries for C_{72} and $B_{36}N_{36}$ calculated by DFT and compared to the Hückel Hamiltonian. The Hückel parameters were fitted from HOMO−6 to LUMO for the carbon cage and from HOMO−6 to LUMO+2 for the BN cage. The HOMO and LUMO are between the two vertical spaces.

C_{72} DFT		Hückel		$B_{36}N_{36}$ DFT+Hückel	DFT	Hückel
Γ	E (eV)	Γ	E (eV)	Γ	E (eV)	E (eV)
T_{1g}	−2.467	E_g	−2.049	E	−0.604	−0.368
E_g	−2.524	T_{1g}	−3.298	T_1	−0.692	−1.034
T_{1u}	−3.257	T_{1u}	−3.673	T_2	−1.259	−1.166
T_{2g}	−5.907	T_{2g}	−5.482	T_2	−6.368	−6.380
T_{2u}	−6.346	T_{2u}	−5.856	T_1	−6.566	−6.512
E_u	−6.764	E_u	−7.105	E	−7.183	−7.179
T_{1u}	−7.460	T_{1u}	−7.452	T_2	−7.397	−7.408
T_{2g}	−7.667	T_{2g}	−7.994	T_2	−7.720	−7.791
T_{1g}	−8.346	T_{1g}	−8.162	T_1	−8.007	−7.915
E_g	−8.426	E_g	−8.450	E	−8.094	−8.133

IX. CONCLUSIONS

The Hückel energies, MOs and their symmetry labels of octahedrally symmetric (4,6) cages have been found for the A_1, A_2 and E representations (the $A+E$ group) by applying a zone-folding procedure, similar to the one applied previously to (3,6) cages.[36] Within the Hückel approximation, most energy levels of the $A+E$ group are twofold degenerate, either imposed by symmetry (E representations), or accidentally (A_1+A_2 couple). For cages with mirror symmetry also accidental fourfold degeneracies occur (E_g+E_u or $A_{1g}+A_{2g}+A_{1u}+A_{2u}$). The two (bonding or antibonding) energy levels closest to energy zero from the $A+E$ group are both E representations for leapfrog cages, while the closest energy level of nonleapfrogs of type 1 (type 2) is an E representation (A_1+A_2 couple) and the second a A_1+A_2 couple (E representation). The MOs of the $A+E$ group close to energy zero have a low density at the squares.

It should be noted that the zone-folding technique cannot be extended to cages with higher-order defects, such as pentagons and heptagons. The reason is that unfolding such structures cannot lead to a regular tessellation of the graphite sheet.

It follows from numerical Hückel calculations that the HOMO-LUMO gap of leapfrog cages is bigger than that of nonleapfrog cages type 1, which is itself bigger than that of type 2. The gap is primarily dependent on the size of the cage and less on the chiral angle. HOMO and HOMO−1 of leapfrog cages are both of T_2 symmetry while LUMO and LUMO+1 are both of T_1 symmetry. HOMO and LUMO of nonleapfrog cages are of T_1 and T_2 symmetry, respectively. MOs of the T group close to energy zero are enhanced in the neighborhood of some of the squares.

The Hückel model gives satisfactory results for both carbon and BN cages, when compared to the more sophisticated DFT method.

ACKNOWLEDGMENTS

Financial support from the Belgian Government through the Concerted Action Scheme (GOA) and from the KULeuven Research Council (BOF) is gratefully acknowledged.

[1] E. E. B. Campbell, P. W. Fowler, D. Mitchell, and F. Zerbetto, Chem. Phys. Lett. **250**, 544 (1996).
[2] T. G. Schmalz, W. A. Seitz, D. J. Klein, and G. E. Hite, J. Am. Chem. Soc. **110**, 1113 (1988).
[3] Y.-D. Gao and W. C. Herndon, J. Am. Chem. Soc. **115**, 8459 (1993).
[4] D. Babić and N. Trinajstić, Chem. Phys. Lett. **237**, 239 (1995).
[5] J. Aihara, J. Chem. Soc., Faraday Trans. **91**, 4349 (1995).
[6] P. W. Fowler, T. Heine, D. E. Manolopoulos, D. Mitchell, G. Orlandi, R. Schmidt, G. Seifert, and F. Zerbetto, J. Phys. Chem. **100**, 6984 (1996).
[7] M. C. Domene, P. W. Fowler, D. Mitchell, G. Seifert, and F. Zerbetto, J. Phys. Chem. A **101**, 8339 (1997).
[8] R. O. Jones and G. Seifert, Phys. Rev. Lett. **79**, 443 (1997).
[9] R. Jones, J. Chem. Phys. **110**, 5189 (1999).
[10] X. Zhao, Z. Slanina, M. Ozawa, E. Osawa, P. Deota, and K. Tanabe, Fullerene Sci. Technol. **8**, 595 (2000).
[11] W. Qian, M. D. Bartberger, S. J. Pastor, K. N. Houk, C. L. Wilkins, and Y. Rubin, J. Am. Chem. Soc. **122**, 8333 (2000).
[12] K. Niedenzu and J. W. Dawson, *Boron-Nitrogen Compounds* (Springer-Verlag, Berlin, 1965).
[13] O. A. Golikova, Phys. Status Solidi A **51**, 11 (1979).
[14] W. Kratschmer, L. D. Lamb, K. Fostiropoulos, and D. R. Huffman, Nature (London) **347**, 354 (1990).
[15] N. G. Chopra, R. J. Luyken, K. Cherrey, V. H. Crespi, M. L. Cohen, S. G. Louie, and A. Zettl., Science **269**, 966 (1995).
[16] A. Loiseau, F. Willaime, N. Demoncy, G. Hug, and H. Pascard, Phys. Rev. Lett. **76**, 4737 (1996).
[17] O. Stephan, Y. Bando, A. Loiseau, F. Willaime, N. Shramchenko, T. Tamiya, and T. Sato, Appl. Phys. A: Mater. Sci. Process. **67**, 107 (1998).
[18] D. Golberg, Y. Bando, O. Stephan, and K. Kurashima, Appl. Phys. Lett. **73**, 2441 (1998).
[19] P. W. Fowler, K. M. Rogers, G. Seifert, M. Terrones, and H. Terrones, Chem. Phys. Lett. **299**, 359 (1999).
[20] H. Y. Zhu, D. J. Klein, W. A. Seitz, and N. H. March, Inorg. Chem. **34**, 1377 (1995).
[21] H. Y. Zhu, T. G. Schmalz, and D. J. Klein, Int. J. Quantum Chem. **63**, 393 (1997).
[22] M. L. Sun, Z. Slanina, and S. L. Lee, Chem. Phys. Lett. **233**, 279 (1995).
[23] Z. Slanina, M. L. Sun, and S. L. Lee, Nanostruct. Mater. **8**, 623 (1997).
[24] I. Silaghi-Dumitrescu, F. Lara-Ochoa, P. Bishof, and I. Haiduc, J. Mol. Struct.: THEOCHEM **367**, 47 (1996).
[25] S. S. Alexandre, M. S. C. Mazzoni, and H. Chacham, Appl. Phys.

Lett. **75**, 61 (1999).
[26] H. Wu, X. Xiaohong, J. Haijun, Z. Fuqiang, and J. Jianfeng, Chin. Sci. Bull. **48**, 1102 (2003).
[27] G. Seifert, P. W. Fowler, D. Mitchell, D. Porezag, and T. Frauenheim, Chem. Phys. Lett. **268**, 352 (1997).
[28] K. M. Rogers, P. W. Fowler, and G. Seifert, Chem. Phys. Lett. **332**, 43 (2000).
[29] I. V. Stankevich, A. L. Chistyakov, and E. G. Galpern, Russ. Chem. Bull. **42**, 1634 (1993).
[30] D. L. Strout, Chem. Phys. Lett. **383**, 95 (2004).
[31] S. S. Alexandre, H. Chacham, and R. W. Nunes, Phys. Rev. B **63**, 045402 (2001).
[32] P. W. Fowler, T. Heine, D. Mitchell, R. Schmidt, and G. Seifert, J. Chem. Soc., Faraday Trans. **92**, 2197 (1996).
[33] F. Jensen and H. Toftlund, Chem. Phys. Lett. **201**, 89 (1993).
[34] M. Dresselhaus, G. Dresselhaus, and P. Eklund, *Science of Fullerenes and Carbon Nanotubes* (Academic, New York, 1994).
[35] A. Ceulemans, L. F. Chibotaru, S. A. Bovin, and P. W. Fowler, J. Chem. Phys. **112**, 4271 (2000).
[36] A. Ceulemans, S. Compernolle, A. Delabie, K. Somers, L. F. Chibotaru, P. W. Fowler, M. J. Marganska, and M. Szopa, Phys. Rev. B **65**, 115412 (2002).
[37] A. Streitweiser, *Molecular Orbital Theory* (Wiley, New York, 1961), Chap. 5.
[38] P. W. Fowler and J. I. Steer, J. Chem. Soc. Dalton Trans. **1997**, 1403 (1997).
[39] P. W. Fowler and A. Ceulemans, J. Phys. Chem. **99**, 508 (1995).
[40] A (2,6) cage has in general three "digons" and $v_{(2,6)}/2-1$ hexagons. A digon consists of two bonds between the same *two* atoms and hence in the connectivity matrix the corresponding value will be two rather than one.
[41] The C_3 axes are of course not present in the three-dimensional form of the folded torus.
[42] P. R. Wallace, Phys. Rev. **71**, 622 (1947).
[43] D. M. Cvetković, M. Doob, and H. Sachs, *Spectra of Graphs: Theory and Application* (Academic, New York, 1979).
[44] M. J. S. Dewar, *The Molecular Orbital Theory of Organic Chemistry* (McGraw-Hill, Inc., New York, 1969), pp. 200–202.
[45] S. Compernolle and A. Ceulemans, J. Phys. Chem. A **109**, 2689 (2005).
[46] A. Schäfer, H. Horn, and R. Ahlrichs, J. Chem. Phys. **97**, 2571 (1992).
[47] R. Ahlrichs, M. Bär, M. Häser, H. Horn, and C. Kölmel, Chem. Phys. Lett. **162**, 165 (1989).